Supplementary Materials

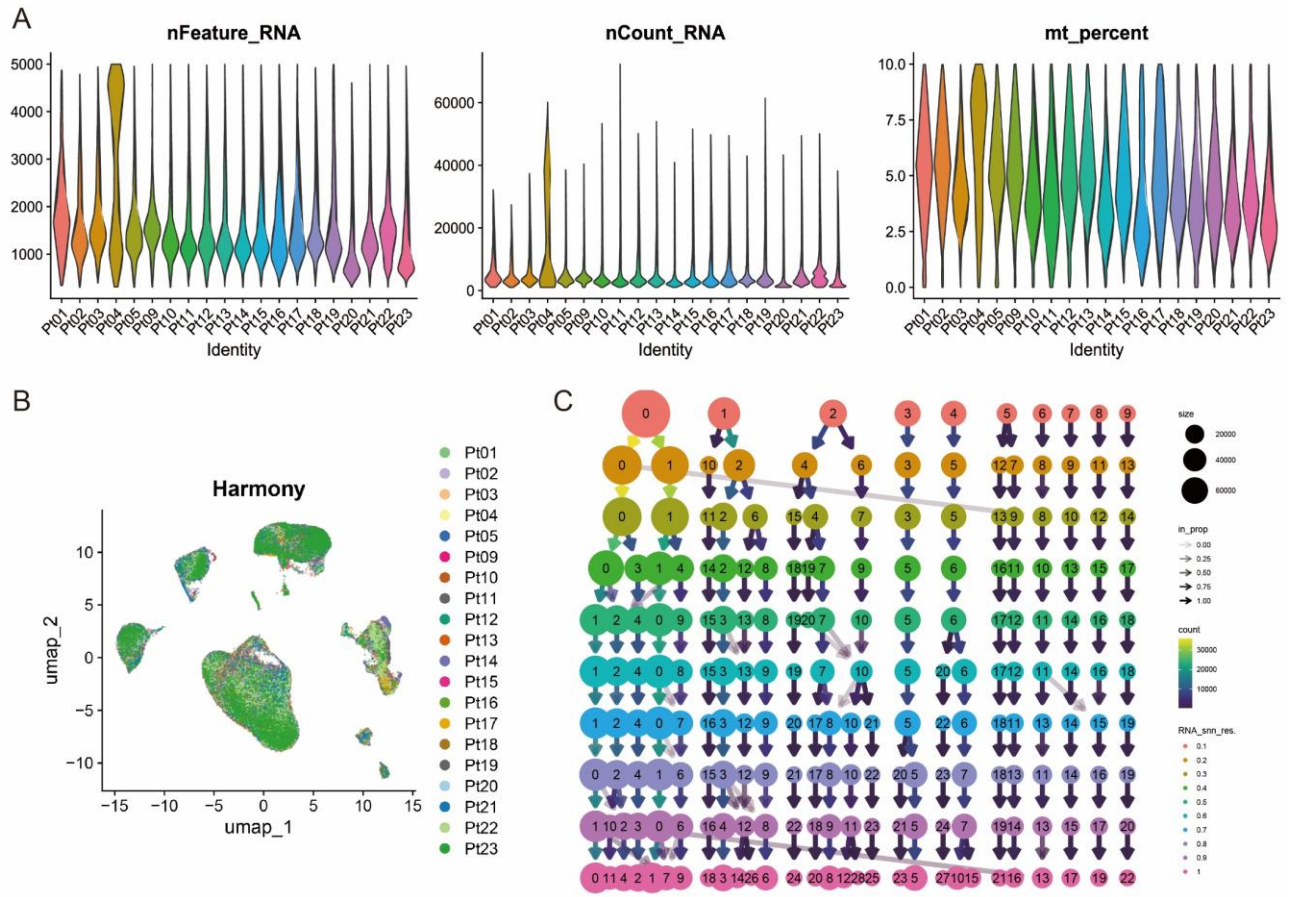

Supplementary Figure 1. Quality control metrics and batch effect correction in single-cell RNA sequencing data.

(A) Violin plots showing quality control metrics across patient samples, including nFeature_RNA (detected genes per cell), nCount_RNA (total UMI counts), and mt_percent (mitochondrial gene percentage). **(B)** UMAP visualization after Harmony batch correction demonstrates effective integration of cells from 20 patient samples (Pt01-Pt23). **(C)** Alluvial plot illustrating clustering stability across different resolution parameters, with node size representing cell count and arrows indicating cluster relationships.

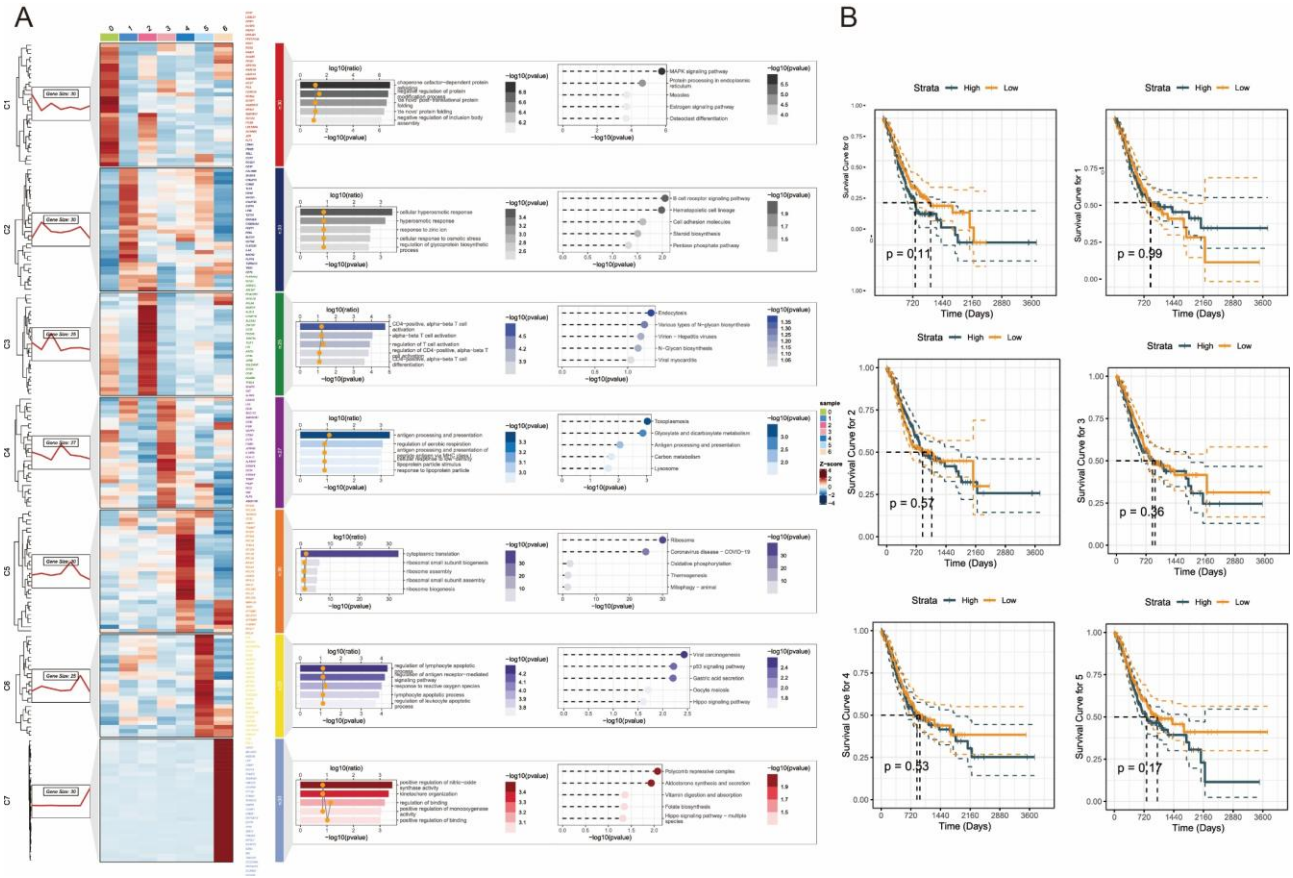

Supplementary Figure 2. Weighted gene co-expression network analysis reveals functional modules and their prognostic associations.

(A) Heatmap displaying gene expression patterns with hierarchical clustering identifying distinct co-expression modules (color bars on the left). Each module is functionally characterized through GO and KEGG enrichment analysis. **(B)** Kaplan-Meier survival curves for representative gene modules, stratifying patients into high and low expression groups. Most modules show no significant prognostic associations ($p > 0.05$).

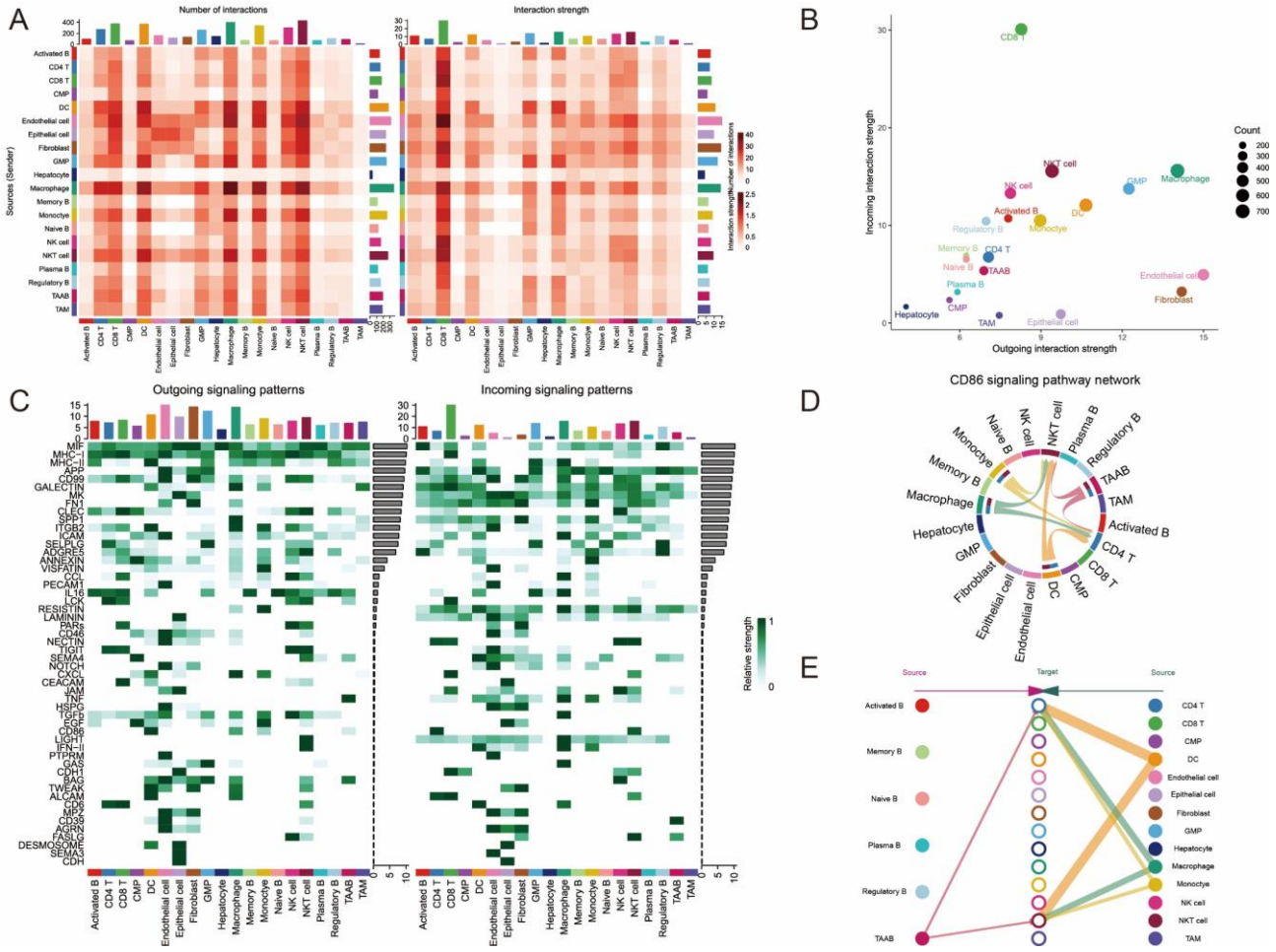

Supplementary Figure 3. Cell-cell communication landscape in the gastric cancer microenvironment.

(A) Heatmaps showing the number and strength of interactions between cell types. **(B)** Scatter plot summarizing incoming and outgoing interaction strength for each cell type, with bubble size representing interaction count. **(C)** Heatmaps displaying outgoing and incoming signaling patterns for specific ligand-receptor pairs across cell populations. **(D)** Chord diagram illustrating the CD86 signaling pathway network, highlighting communication between immune cell subsets. **(E)** Sankey diagram depicting specific signaling interactions between B cell subsets (Activated B, Memory B, Naive B, Plasma B, Regulatory B, and TAAB) and other cell types including T cells, dendritic cells, epithelial cells, fibroblasts, and macrophages.

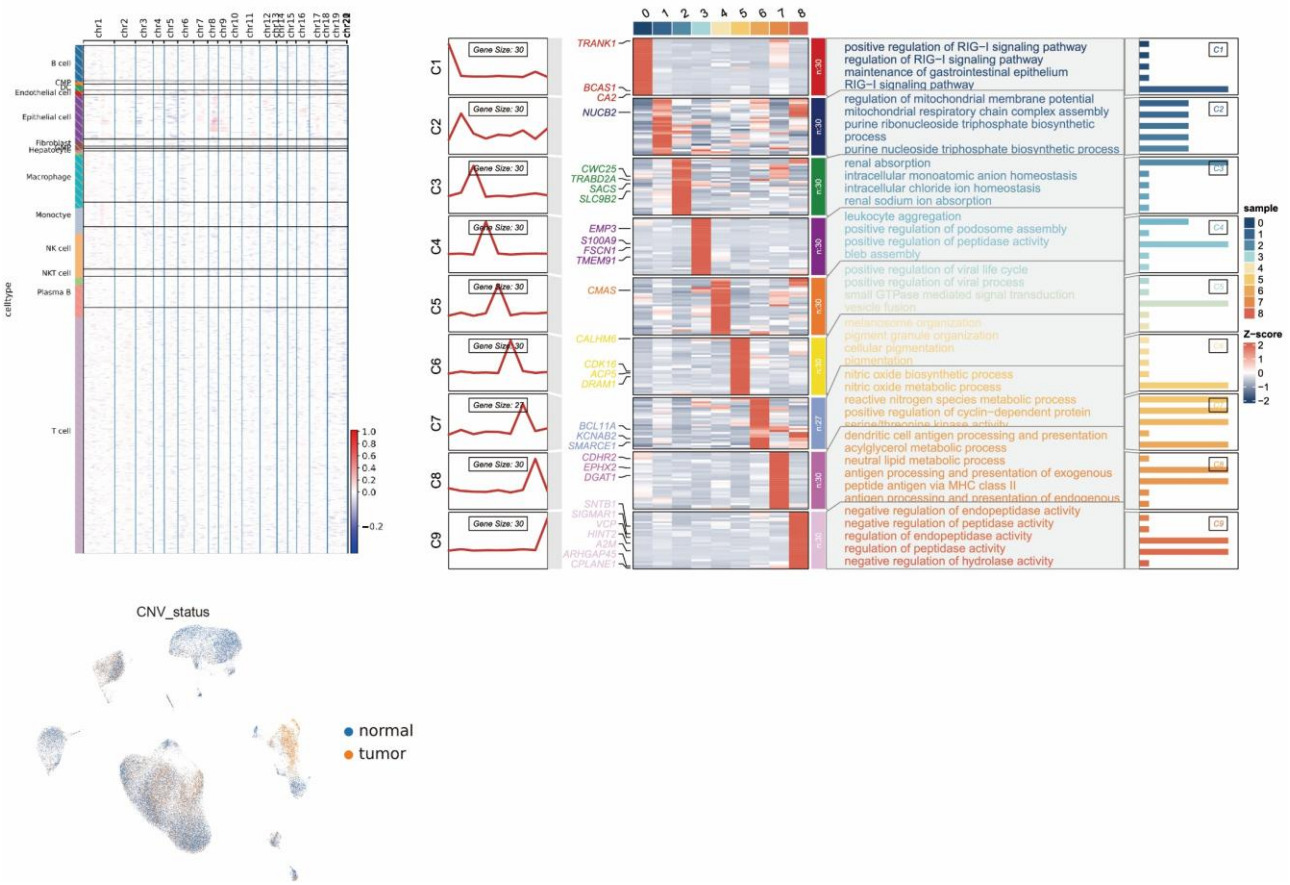

Supplementary Figure 4. Cell type distribution and functional gene clustering analysis.

Heatmap showing cell type proportions across patient samples, including B cells, endothelial cells, epithelial cells, fibroblasts, macrophages, monocytes, NK cells, NKT cells, plasma B cells, and T cells. Nine gene clusters (C1-C9) identified through expression profiling display distinct biological processes, with representative genes labeled. UMAP visualization distinguishes normal (blue) and tumor (orange) cells based on CNV status.

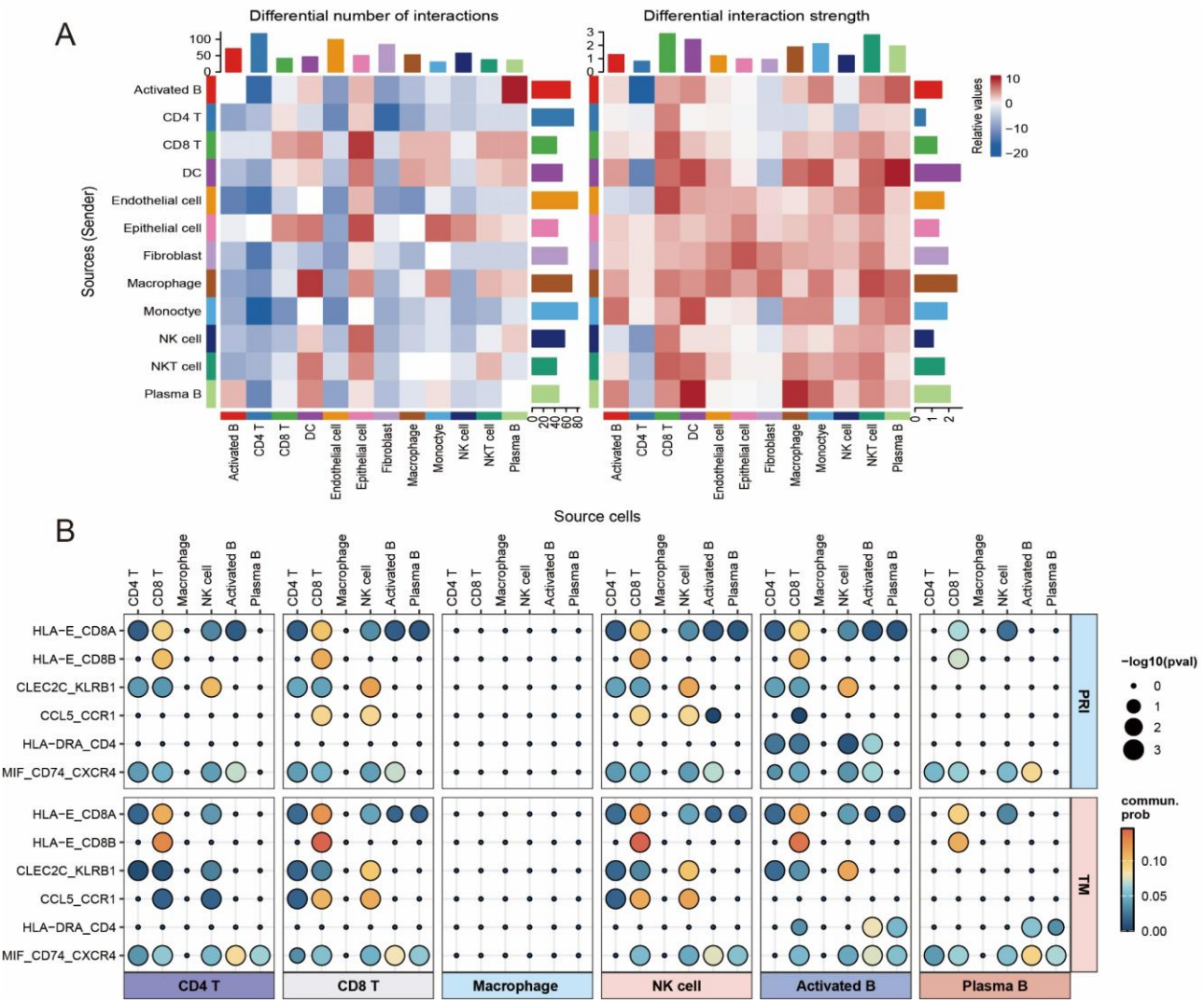

Supplementary Figure 5. Differential cell-cell communication patterns across tissue types.

(A) Heatmaps showing differential number and strength of interactions between cell types. Bar plots indicate the total differential interactions for each cell type. **(B)** Bubble plots displaying the communication probability of specific ligand-receptor pairs across different cell types in PRI and LM, with bubble size representing significance and color indicating communication probability. Key interactions are highlighted including MIF-CD74-CXCR4 signaling across multiple immune cell populations.

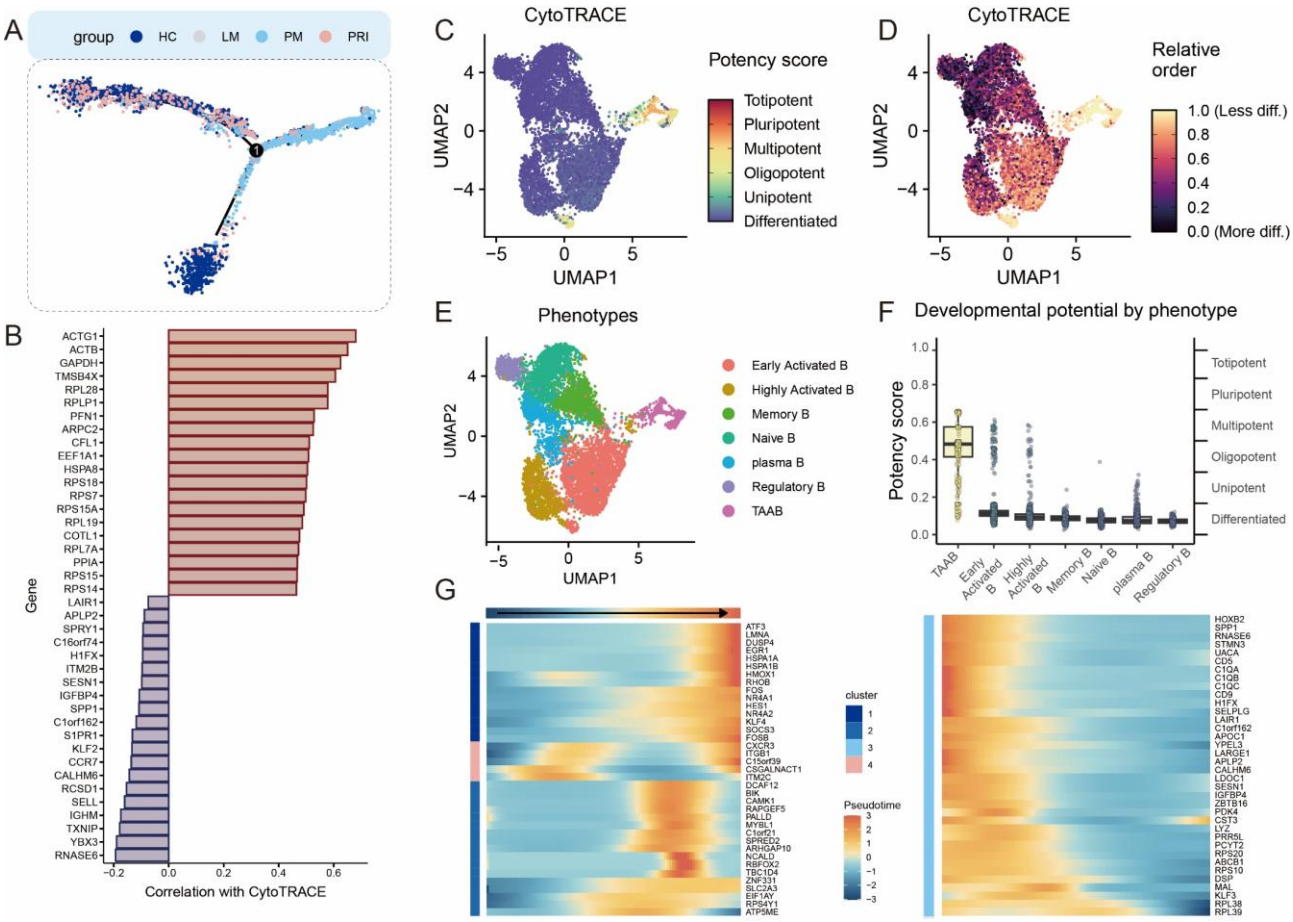

Supplementary Figure 6. CytoTRACE analysis and gene expression dynamics across tissue types and B cell phenotypes.

(A) UMAP visualization showing distribution of cells from different tissue sources including HC, LM, PM and PRI. **(B)** Bar plot displaying genes positively (brown) and negatively (purple) correlated with CytoTRACE scores, indicating their association with cellular differentiation potential. **(C-D)** CytoTRACE analysis mapping potency scores and relative differentiation order, with higher scores indicating stem-like properties and lower scores representing more differentiated states. **(E)** Distribution of B cell phenotypes including Early Activated B, Highly Activated B, Memory B, Naive B, plasma B, Regulatory B, and TAAB. **(F)** Box plots showing developmental potential scores across different B cell phenotypes, with TAAB exhibiting lower differentiation potential. **(G)** Heatmap illustrating gene expression dynamics along pseudotime, with genes clustered into four groups showing distinct temporal patterns.

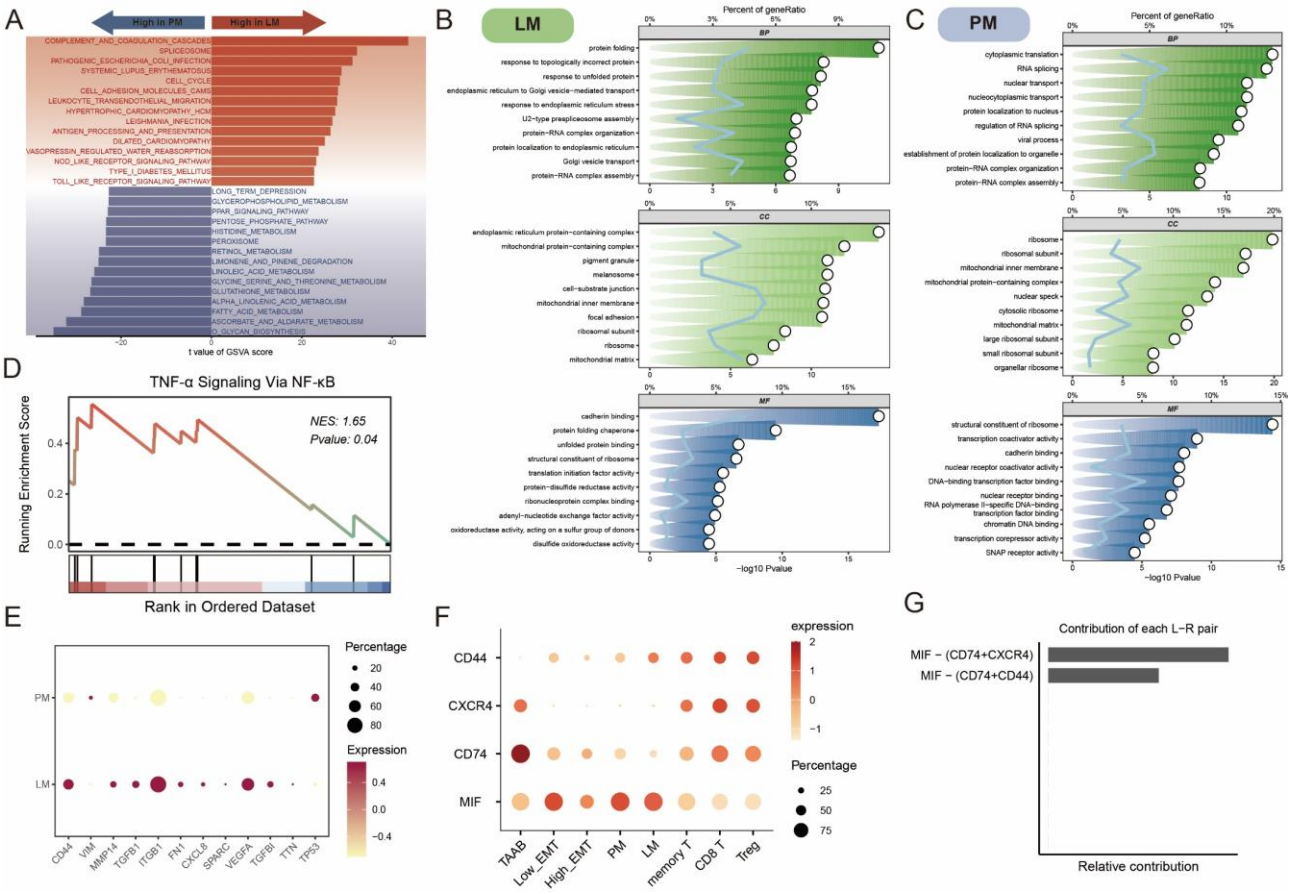

Supplementary Figure 7. Pathway enrichment and ligand-receptor interaction analysis in metastatic sites.

(A) GSVA analysis showing pathways enriched in PM (red) versus LM (blue). **(B-C)** GO enrichment analysis for LM and PM respectively, revealing distinct biological processes, cellular components, and molecular functions. **(D)** GSEA plot demonstrating significant enrichment of TNF-α signaling via NF-κB pathway (NES=1.65, P=0.04). **(E)** Dot plot displaying expression and percentage of key ligands across PM and LM samples. **(F)** Expression of MIF, CD74, CXCR4, and CD44 across different B cell subsets. **(G)** Bar plot showing relative contribution of MIF-(CD74+CXCR4) and MIF-(CD74+CD44) ligand-receptor pairs.

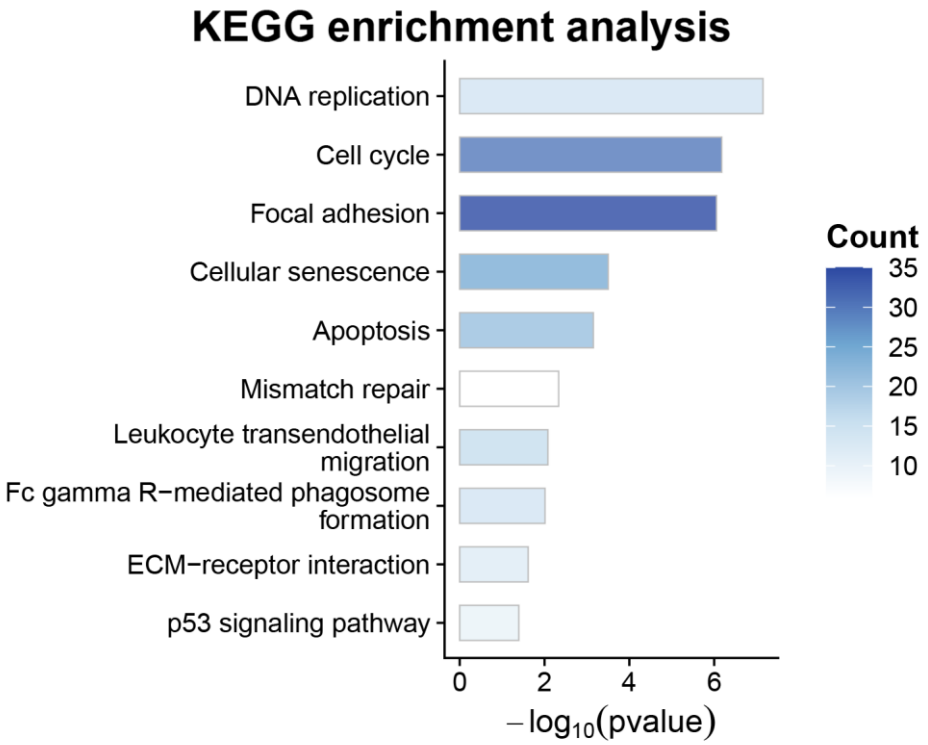

Supplementary Figure 8. KEGG pathway enrichment analysis of the turquoise module genes.